Abdominal Radiology
https://doi.org/10.1007/s00261-020-02755-5

TECHNICAL

Fully automated CT imaging biomarkers of bone, muscle, and fat: correcting for the effect of intravenous contrast

Alberto A. Perez[1] · Perry J. Pickhardt[1,3] · Daniel C. Elton[2] · Veit Sandfort[2] · Ronald M. Summers[2]

Received: 6 July 2020 / Revised: 31 August 2020 / Accepted: 3 September 2020

Abstract

Purpose Fully automated CT-based algorithms for quantifying bone, muscle, and fat have been validated for unenhanced abdominal scans. The purpose of this study was to determine and correct for the effect of intravenous (IV) contrast on these automated body composition measures.

Materials and methods Initial study cohort consisted of 1211 healthy adults (mean age, 45.2 years; 733 women) undergoing abdominal CT for potential renal donation. Multiphasic CT protocol consisted of pre-contrast, arterial, and parenchymal phases. Fully automated CT-based algorithms for quantifying bone mineral density (BMD, L1 trabecular HU), muscle area and density (L3-level MA and M-HU), and fat (visceral/subcutaneous (V/S) fat ratio) were applied to pre-contrast and parenchymal phases. Effect of IV contrast upon these body composition measures was analyzed. Square of the Pearson correlation coefficient (r^2) was generated for each comparison.

Results Mean changes (± SD) in L1 BMD, L3-level MA and M-HU, and V/S fat ratio were 26.7 ± 27.2 HU, 2.9 ± 10.2 cm^2, 18.8 ± 6.0 HU, − 0.1 ± 0.2, respectively. Good linear correlation between pre- and post-contrast values was observed for all automated measures: BMD (pre = 0.87 × post; $r^2 = 0.72$), MA (pre = 0.98 × post; $r^2 = 0.92$), M-HU (pre = 0.75 × post + 5.7; $r^2 = 0.75$), and V/S (pre = 1.11 × post; $r^2 = 0.94$); $p < 0.001$ for all r^2 values. There were no significant trends according to patient age or gender that required further correction.

Conclusion Fully automated quantitative tissue measures of bone, muscle, and fat at contrast-enhanced abdominal CT can be correlated with non-contrast equivalents using simple, linear relationships. These findings will facilitate evaluation of mixed CT cohorts involving larger patient populations and could greatly expand the potential for opportunistic screening.

Keywords Image processing · Opportunistic screening · IV contrast · Bone-mineral-density · Muscular atrophy · Intra-abdominal fat

Introduction

Abdominal CT scans contain robust information on body composition unrelated to the study indication which often goes unused in clinical practice [1]. Fully automated CT-based tools can now use artificial intelligence (AI) algorithms to rapidly and objectively acquire biometric data from these studies to be used in opportunistic screening. Such data can then be used for patient risk stratification and prediction of future adverse events. To date, CT-based AI tools have been validated for the quantification of bone mineral density, liver fat, muscle bulk and density, calcification of the abdominal aorta, and intra-abdominal fat [2–6]. Biometric data acquired from these tools have also been demonstrated to have predictive value comparable to established clinical-based screening tools [7–9].

Importantly, the data from all of the above studies were collected from non-contrast CT studies. While some work has been done to determine the effects of intravenous (IV) contrast on CT-based biometric measures [10–12], evaluation on fully automated AI collected biometric data is

✉ Perry J. Pickhardt
ppickhardt2@uwhealth.org

1 The University of Wisconsin School of Medicine & Public Health, Madison, WI, USA

2 Imaging Biomarkers and Computer-Aided Diagnosis Laboratory, Radiology and Imaging Sciences, National Institutes of Health Clinical Center, Bethesda, MD, USA

3 Department of Radiology, University of Wisconsin School of Medicine & Public Health, E3/311 Clinical Science Center, 600 Highland Ave., Madison, WI 53792-3252, USA

Published online: 18 September 2020

limited. The purpose of this study was to determine and correct for the effect of IV contrast on measures of bone, muscle, and fat, such that previously proposed opportunistic screening techniques could be expanded to contrast-enhanced CT studies.

Methods

Patient cohort and CT protocol

This HIPAA-compliant investigation was approved by the Institutional Review Board at the University of Wisconsin and the Office of Human Subjects Research Protection at the NIH Clinical Center. The requirement for signed informed consent was waived for this retrospective assessment. From a generally healthy, asymptomatic adult cohort of 1250 consecutive individuals undergoing abdominal CT for potential renal donation between February 2010 and January 2017, a final study cohort of 1211 was procured after exclusion of missing or corrupted image data. Basic demographic (age and gender) was collected for these 1211 subjects.

All individuals in the study cohort underwent abdominal CT utilizing a dedicated multiphasic protocol for the purpose of renal donor evaluation. All scans were performed on multidetector-row CT scanners (GE Healthcare, Waukesha, WI), typically with 64×0.625 detector configuration, 120 kV setting, and modulated mA with noise index ranging from 17.0 to 27.5, both based on patient size. A pre-contrast abdominal series was obtained extending from T12-L4. A split-bolus IV contrast technique was used to achieve multiphase dynamic and excretory imaging. An initial injection consisted of 20 ml of nonionic contrast (with 20 ml saline flush) 5 min prior to the multiphasic injection to opacify the upper collecting system. Multiphasic injection consisted of split bolus of 30 ml contrast (and 30 ml saline) at 3 ml/s prior to the arterial/vascular phase acquisition, followed by 100 ml contrast/50 ml saline at 5 ml/s 20 s later for the late portal venous/parenchymal phase acquisition. For this study, only the pre-contrast and parenchymal post-contrast phases were utilized for assessing the automated CT tools described below. For the arterial phase, the partial coverage was inadequate for assessment, and furthermore, this phase is of less interest for use with our automated body composition tools. Series were originally reconstructed as 5 mm slices at 3-mm intervals. The images were retrospectively reformatted to 3 mm slices at 3-mm intervals.

Automated CT biomarkers

The deep-learning and image processing algorithms used in this study were previously developed and tested. The CT-based algorithms are designed to automatically segment and quantify visceral and subcutaneous fat, body wall musculature, and vertebral trabecular bone at specific spinal levels. These have all been trained and tested on separate cohorts not used in the current study [13–17]. Additional validation studies for these tools in a separate patient cohort investigating normative values and changes over time of the algorithm outputs have also been published [3, 5, 6]. These works have all utilized the high-performance computing capabilities of the NIH Biowulf system.

Detailed descriptions of the AI methodology for automated CT-based anatomic tissue segmentation and quantification tools are provided in the above referenced works. Briefly, for bone and fat quantification, feature-based image processing algorithms were used to first identify and segment vertebral levels T12-L5. At the desired vertebral level, the anterior trabecular space is then isolated for BMD measures, as are the visceral and subcutaneous fat compartments. The abdominal wall musculature tool uses a deep-learning algorithm consisting of a modified 3D U-Net for segmentation and analysis at the desired vertebral level.

Based on the prior works [3, 5, 6], it was determined that the L3 level was preferred for muscle assessment and the L1 level was best for both bone and fat measurements. Therefore, for this study, we used the final selected tissue measures applied to the pre- and post-contrast series: L1-level trabecular HU for bone, L3-level abdominal wall muscle HU, L3-level abdominal wall muscle area, and L1-level visceral-to-subcutaneous (V/S) fat ratio. Figure 1 demonstrates typical pre- and post-contrast case examples of these automated measures. Patients who had a failed biomarker measure on pre- and/or post-contrast studies were excluded from analysis of that biomarker, but remained included for analysis of other successfully measured biomarkers.

Statistical analysis

Summary statistics were compiled for biomarker measurements for pre- and post-contrast studies as well as change between the two. Linear least-squares regression analysis was performed to compare pre-and post-contrast biomarker results. After initial data review, a set dependent (pre-contrast) variable intercept of 0 was used for V/S fat ratio, abdominal wall muscle area, and L1 BMD. A least-squares estimated intercept was used for abdominal wall muscle density. As such, r^2 equals the square of the Pearson correlation coefficient between the observed and modeled (predicted) data values of the dependent variable.

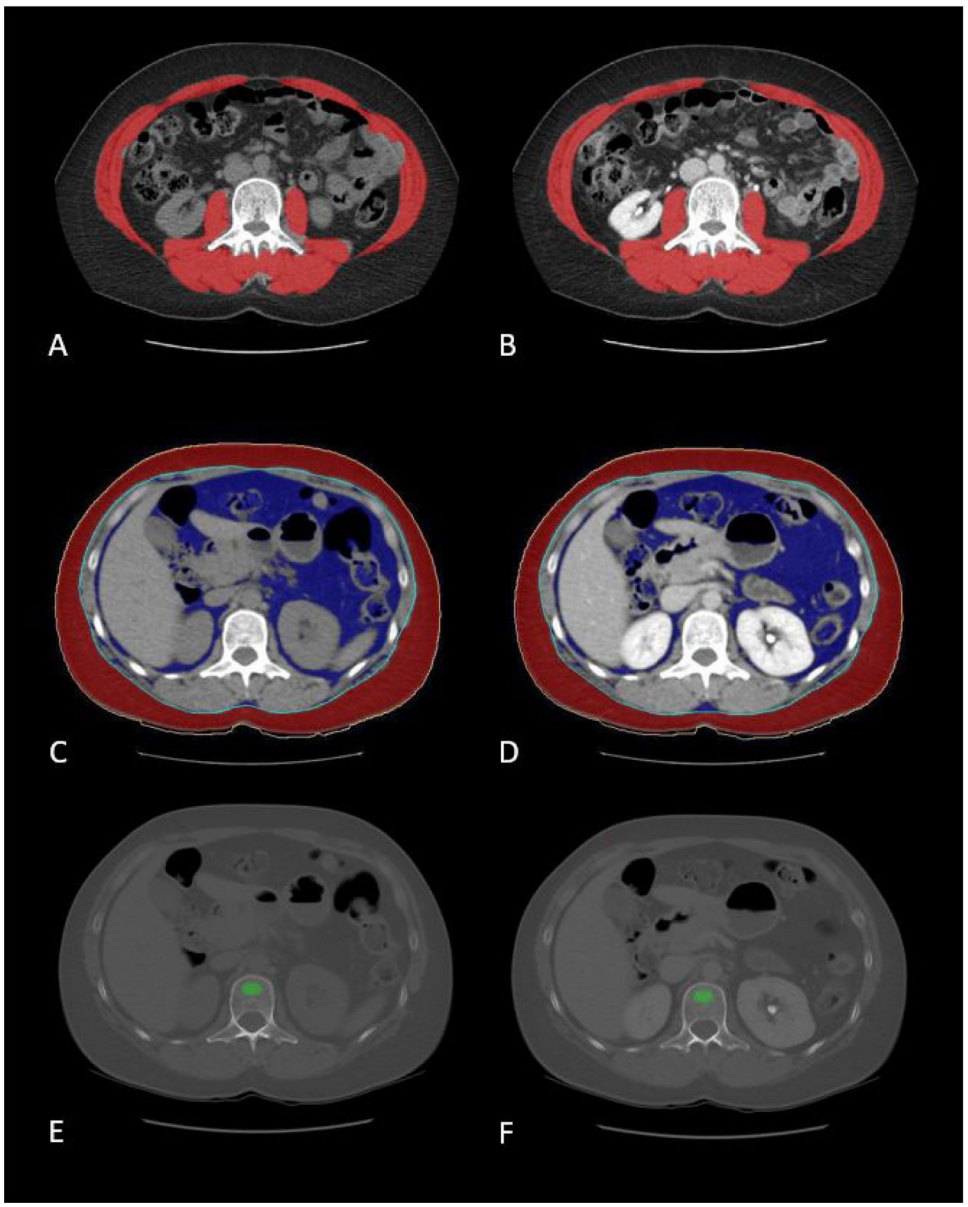

Fig. 1 Composite of CT images demonstrating output from automated algorithms in a 43-year-old woman. Pre-contrast and post-contrast image pairs are shown for L3-level muscle (red) segmentation (**a** and **b**), L1-level visceral (blue) and subcutaneous (red) fat segmentation (**c** and **d**), and L1 trabecular sampling (**e** and **f**, green ROI)

Results

Patient demographics

Average age of patients was 45.2 years with a SD of 12.5 (minimum 18; maximum 76 years); 733 of the total 1211 patients were female (478 males). Age and gender were not meaningful, independent predictors of change in CT-based biomarker measurements between pre- and post-contrasted studies for any of the body composition measures in the cohort ($n = 1211$).

Visceral and subcutaneous fat area

Pre- and post-contrast visceral and subcutaneous fat area data were successfully acquired for 1204 of the 1211 subjects in the cohort (99.4%). An average ($\pm$ SD) of 353.8 ± 286.5 mm^2 and 282.7 ± 256.3 mm^2 was measured for pre- and post-contrast visceral fat areas, respectively, representing an average ($\pm$ SD) change of -71.1 ± 55.1 mm^2, or a 25.4% average decrease in area measured on contrasted studies. An average ($\pm$ SD) of 454.2 ± 276.9 mm^2 and 421.8 ± 271.0 mm^2 was measured for pre- and post-contrast subcutaneous fat

Fig. 2 Pre-contrast vs. post-contrast fat measurement data. Scatterplot shows the strong linear correlation for pre- and post-contrast automated visceral-to-subcutaneous (V/S) fat ratio

areas, respectively, representing an average (± SD) change of 32.4 ± 33.9 mm^2, or a 9.4% average decrease in area measured on contrasted studies. The relationship of pre- and post-contrast visceral fat area (V_{Pre} and V_{Post}) was modeled with the linear correlation of $V_{Pre} = 1.18 \times V_{Post}$ ($r^2 = 0.96$; $p = < 0.001$). The relationship of pre- and post-contrast subcutaneous fat area (S_{Pre} and S_{Post}) was modeled with the linear correlation of $S_{Pre} = 1.06 \times S_{Post}$ ($r^2 = 0.98$; $p = < 0.001$).

Average (± SD) V/S ratio was 0.87 ± 0.73 in pre-contrast studies and 0.74 ± 0.68 in post-contrast studies. The average change (± SD) after contrast was − 0.13 ± 0.17, representing a 17% decrease on average after contrast. Figure 2 shows the relationship of pre- and post-contrast V/S ratio (V/S_{Pre} and V/S_{Post}), modeled with the linear correlation of $V/S_{Pre} = 1.11 \times V/S_{Post}$ ($r^2 = 0.97$; $p = < 0.001$).

Muscle area and density

Pre- and post-contrast L3-level muscle area data were successfully acquired for 1205 of the 1211 subjects in the cohort (99.5%). An average (± SD) of 141.0 ± 36.8 mm^2 and 143.8 ± 37.7 mm^2 was measured for pre- and post-contrast areas, respectively, representing an average (± SD) change of 2.9 ± 10.2 mm^2, or a 2.4% average increase with contrasted studies. The relationship of pre-contrast muscle area ($M\text{-}Area_{Pre}$) and post-contrast muscle area ($M\text{-}Area_{Post}$) is shown in Fig. 3a, resulting in a linear correlation of $M\text{-}Area_{Pre} = 0.98 \times M\text{-}Area_{Post}$ ($r^2 = 0.92$; $p = < 0.001$).

Pre- and post-contrast L3-level muscle density data were acquired for 1205 subjects in the cohort 99.5%. An average (± SD) of 32.7 ± 10.6 HU and 51.5 ± 12.3 HU was measured for pre- and post-contrast attenuation, respectively, representing an average (± SD) change of 18.8 ± 6.0 HU, or a 77.3% average increase on contrasted studies. The relationship of pre-contrast muscle attenuation ($M\text{-}HU_{Pre}$) and post-contrast muscle attenuation ($M\text{-}HU_{Post}$) is shown in Fig. 3b with a linear correlation of $M\text{-}HU_{Pre} = 0.75 \times M\text{-}HU_{Post} + 5.7$ ($r^2 = 0.75$; $p = < 0.001$). As HU values less than zero are physiologically reasonable in muscle with more extensive

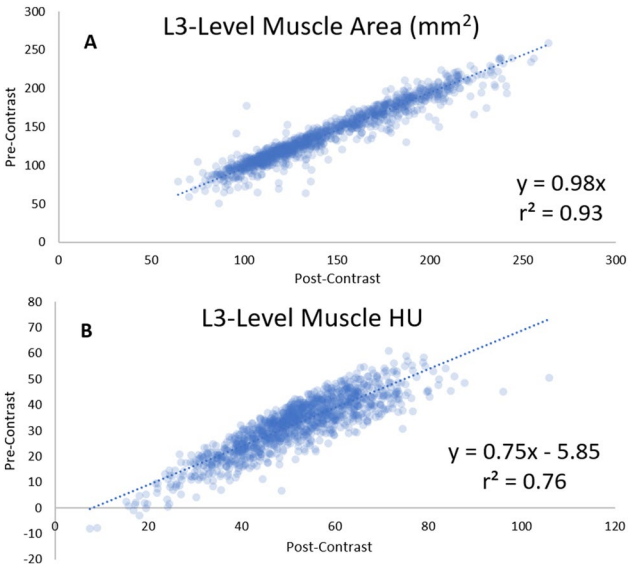

Fig. 3 Pre-contrast vs. post-contrast muscle measurement data. Scatterplots show the correlation between pre- and post-contrast automated L3-level muscle area (**a**) and attenuation values (**b**). Not surprisingly, the linear correlation is stronger for area, but was also apparent for attenuation values. Muscle HU was the one measure that necessitated a non-zero intercept

fatty involution, an estimated y-intercept was used for the linear regression.

Bone mineral density

Pre- and post-contrast BMD data were acquired for 1187 subjects in the final cohort (98.0%). An average (± SD) of 186.1 ± 47.1 HU and 212.8 ± 51.7 HU was measured for pre- and post-contrast attenuation, respectively, representing an average (± SD) change of 26.7 ± 27.2 HU, or a 15.8% average increase with contrasted studies. The relationship of L1 trabecular bone pre-contrast attenuation ($B\text{-}HU_{Pre}$) and post-contrast attenuation ($B\text{-}HU_{Post}$) is shown in Fig. 4 with the

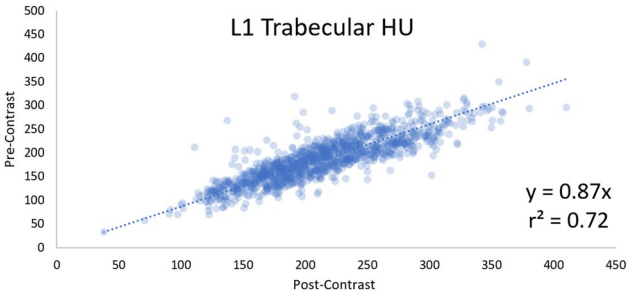

Fig. 4 Pre-contrast vs. post-contrast BMD measurement data. Scatterplots show the correlation between pre- and post-contrast automated L1 trabecular attenuation values

linear correlation of D-HU_{Pre} = 0.87 × D-HU_{Post} (r^2 = 0.72; p = < 0.001).

Analysis of segmentation errors

Qualitative visual review of the automated CT tools in the uncommon outlier cases usually revealed errors in segmentation as the underlying reason for the discrepancy. Common segmentations errors included: for muscle, missing parts of the muscles or getting the L3 level incorrect; for fat, inability to find the abdominal wall and getting the L1 level incorrect; and for bone, erroneous placement of the ROI within the vertebral body and getting the L1 level incorrect; for all tools, patient motion or inaccurate registration between pre- and post-contrast series. Examples of such errors are shown in Fig. 5.

Discussion

Comparing automated CT biomarker measurements on pre- and post-contrast studies, we found that simple linear correlations effectively accounted for the population-based effects of IV contrast for the various muscle, fat, and bone measures of interest. Specifically, V/S fat area ratios (r^2 = 0.97), L3 muscle area (r^2 = 0.92), muscle density (r^2 = 0.75), and L1 trabecular density (r^2 = 0.72) all demonstrated a clear linear trend. The main motivation for our study was to see if a "correction" for the effect of IV contrast would allow us to combine unenhanced and enhanced CT scans for performing large population-based predictive studies using these CT biomarkers of body composition. Such corrections might also be useful at the individual patient level if these opportunistic measures are to be used prospectively for risk

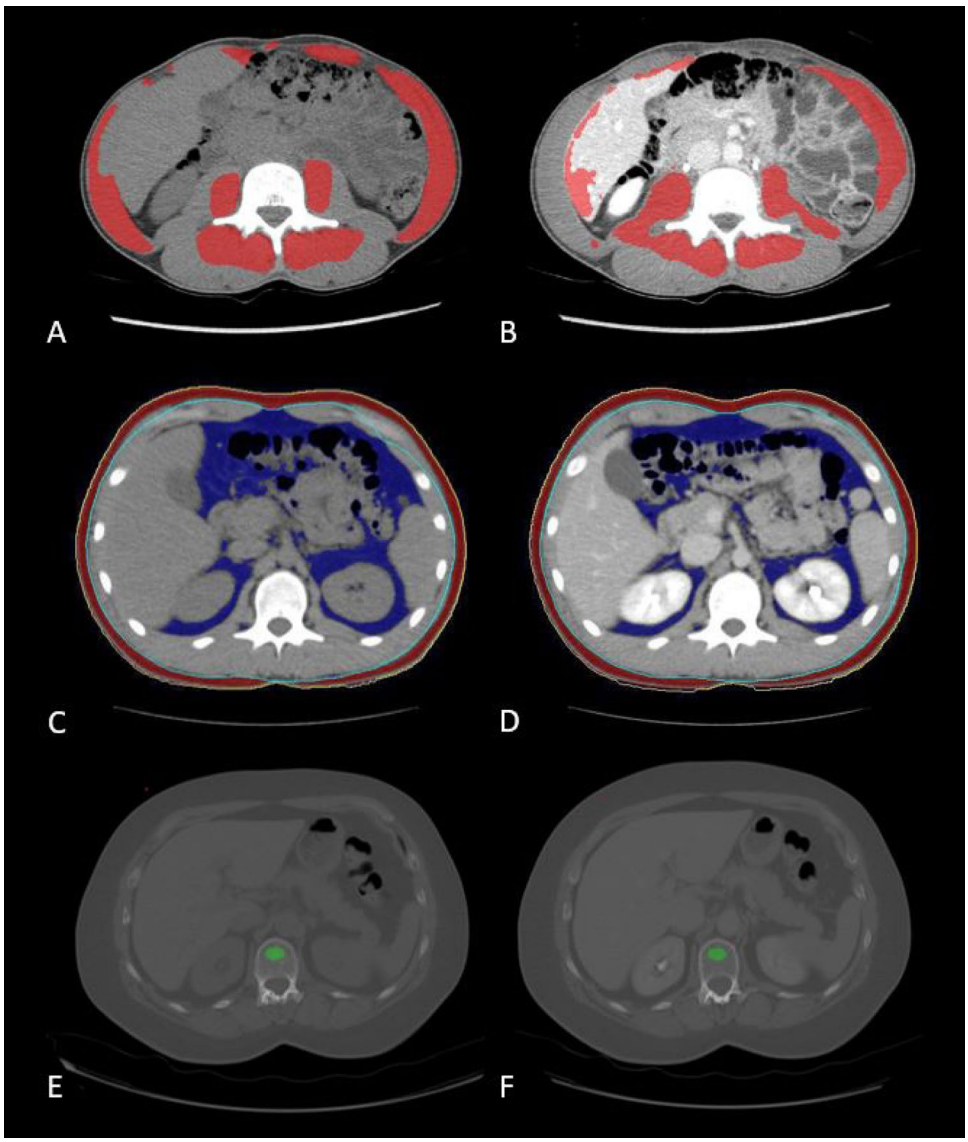

Fig. 5 Case examples of discordant/outlier results between pre- and post-contrast. Pre-contrast (**a**) and post-contrast (**b**) example of the muscle tool shows obvious segmentation errors. Pre-contrast (**c**) and post-contrast (**d**) example of the fat tool shows expected segmentation, but the amount of visceral fat has shifted at the anatomic L1 level relative to other structures, presumably related to respiratory differences. IV contrast also impacts visceral fat segmentation more than subcutaneous fat. Pre-contrast (**e**) and post-contrast (**f**) example of the L1 trabecular bone tool shows pre-contrast placement of the ROI near the endplate, including cortical bone that resulted in a 46.4 HU increase over the properly placed post-contrast trabecular ROI

assessment in the future. However, visual confirmation of correct automated segmentation, including level, would be an important quality assurance step for individual patient care.

The fact that such a straightforward linear correction is sufficient to account for the effect of IV contrast on these automated measures was somewhat serendipitous, both for the area-based and HU-based assessments. For the area-based measures of muscle and fat, one might expect that no correction at all is needed, since the underlying amount of tissue being assessed is of course unchanged. Indeed, the measured difference in L3-level muscle area was only on the order of 2% on average. However, the mean post-contrast decrease in L1-level visceral fat was substantially larger, at about 25%, presumably due to the impact of contrast enhancement of surrounding organs and vessels at the fat interface, affecting the regions of fat thresholding. Not surprisingly, the effect on subcutaneous fat area was less (< 10%), but still much greater than the effect on muscle area. Nonetheless, the changes in visceral fat, subcutaneous fat, and V/S ratio were all linear in nature for the study cohort. Measurable changes in post-contrast attenuation values of the vascularized structures of muscle and trabecular bone (in HU) were more expected, but the reasonably good linear correlation was not. In addition, the lack of need for a non-zero intercept for L1 trabecular HU was unexpected. The increased muscle enhancement associated with higher pre-contrast HU values may reflect more vascularized muscle without fatty atrophy or myosteatosis.

Spatial misregistration due to breath-hold differences between the pre- and post-contrast series is another potential source of variability in biomarker measurement. Relative motion would be more expected to affect visceral fat compared with muscle or bone. This may also help to further explain the greater mean differences observed in visceral fat measures. Although vertebral bone is the least likely to shift due to respiratory changes, the L1 trabecular HU ROI is much smaller and more sensitive to position, such as proximity to the vertebral endplate. This may help to explain the relative increase in outlier measures for BMD. These two issues are visually apparent in the cases shown in Fig. 5.

Although we are not aware of other pre- and post-contrast investigations involving automated CT tools, prior studies utilizing manual ROI attenuation measurements for assessing post-contrast changes in muscle and trabecular bone have been reported. One study assessing the paraspinal and psoas muscles on pre- and multiphase post-contrast studies showed a significant increase in attenuation after contrast administration, which was greatest in the delayed (parenchymal) phase [10]. Additionally, this manual study showed a significant increase in L4 trabecular bone. Another study using manual ROI placement on pre- and post-contrast CT images showed an average increase in L1 trabecular attenuation of 11.2 HU after contrast, but with relatively wide variability [11]. Yet another manual ROI study showed the effect of contrast on L1 trabecular bone attenuation on arterial and portal venous phases, and noted that this could affect BMD assessment [12].

The need for validating these fully automated biometric tools on post-contrast CT scans is clear, based on the initial validation [3, 5, 6] and predictive works [7–9] to date using only unenhanced CT scans. In conjunction with automated CT-based tools for quantifying abdominal aortic calcification and liver fat [2, 4], the automated muscle, fat, and bone tools evaluated herein have contributed to studies demonstrating their predictive value for future osteoporotic fractures, cardiovascular events and mortality, and metabolic syndrome [1, 7–9]. All of the biomarker data for these previous studies, however, were collected from non-contrast CT examinations. The ability to apply these tools to population-based studies involving a mix of unenhanced and contrast-enhanced CT scans would greatly expand their opportunistic potential. Ongoing work is focusing on the effects of IV contrast on the automated abdominal aortic calcium and liver HU tools. For quantifying aortic calcium on post-contrast CT, the impact of the immediately adjacent blood pool enhancement presents additional technical challenges. For quantifying liver fat content, preliminary investigation suggests that a simple linear correction may be insufficient.

To be effectively utilized at the patient level, such as for prospective opportunistic risk stratification on CT scans performed for other clinical indications, visual assessment and confirmation of appropriate automated segmentations will be indicated. This quality assurance step would apply to both unenhanced and contrast-enhanced CT scans. For post-contrast correction, population averages assuming linear correlation are meaningless for individualized care if the automated measurement represents a flawed outlier. As such, a dashboard display of automatically segmented measures of body composition should be available to the radiologist at the time of prospective interpretation.

We acknowledge limitations to our study. The patient cohort was solely comprised of healthy outpatient adults. Although this represents an appropriate well-controlled group for initial assessment of IV contrast effects, our findings should eventually be extended to a broader scope of patients, including symptomatic and diseased cohorts. We utilized a more delayed parenchymal post-contrast phase, and not the standard portal venous phase. While this ensured ample time to measure the full effect of IV contrast, and avoided situations where the portal venous phase is obtained too early, it may impact generalizability. A minority of cases were scanned at non-120 kV settings; however, we felt this was insufficient for formal subanalysis, and the overall correlations were deemed to be adequate. Finally, the automated CT-based algorithms failed in a minority of cases, and

outliers related to segmentation error were observed in other cases. Segmentation errors related to the BMD tool were most frequent. Over time, continued refinements to these AI algorithms are expected to further reduce the error rate. This along with further testing could allow for conversion of contrasted biomarkers to their non-contrast equivalent.

In conclusion, we have shown that fully automated CT-based quantitative tissue measures of bone, muscle, and fat at contrast-enhanced abdominal CT correlate with non-contrast equivalents using simple linear relationships. This finding will facilitate the evaluation of mixed CT cohorts involving larger patient populations and could greatly expand the potential for both population-based and individualized opportunistic screening.

Acknowledgements This research was supported in part by the Intramural Research Program of the National Institutes of Health Clinical Center, and utilized the high-performance computing capabilities of the NIH Biowulf cluster. We thank NVIDIA for GPU card donation.

Compliance with ethical standards

Conflict of interest Dr. Pickhardt serves is an advisor to Bracco and Zebra and is a shareholder in SHINE, Elucent, and Cellectar; Dr. Summers receives royalties from iCAD, PingAn, Philips, ScanMed and Translation Holdings, and research support from PingAn (CRADA) and NVIDIA (GPU card donations).

References

1. Pickhardt PJ, Graffy PM, Lubner MG, Summers RM. Opportunistic screening at abdominal CT using automated biomarkers: adding value beyond the clinical indication. RadioGraphics (submitted).
2. Graffy PM, Liu J, O'Connor S, Summers RM, Pickhardt PJ. Automated segmentation and quantification of aortic calcification at abdominal CT: application of a deep learning-based algorithm to a longitudinal screening cohort. Abdom Radiol 2019;44:2921–9.
3. Graffy PM, Liu J, Pickhardt PJ, Burns JE, Yao J, Summers RM. Deep learning-based muscle segmentation and quantification at abdominal CT: application to a longitudinal adult screening cohort for sarcopenia assessment. The British journal of radiology 2019:20190327.
4. Graffy PM, Sandfort V, Summers RM, Pickhardt PJ. Automated Liver Fat Quantification at Nonenhanced Abdominal CT for Population-based Steatosis Assessment. Radiology 2019:190512.
5. Lee SJ, Liu J, Yao J, Kanarek A, Summers RM, Pickhardt PJ. Fully automated segmentation and quantification of visceral and subcutaneous fat at abdominal CT: application to a longitudinal adult screening cohort. The British journal of radiology 2018;91:20170968.
6. Pickhardt PJ, Lee SJ, Liu JM, et al. Population-based opportunistic osteoporosis screening: Validation of a fully automated CT tool for assessing longitudinal BMD changes. The British journal of radiology 2019;92.
7. Pickhardt PJ, Graffy PM, Zea R, et al. Automated CT biomarkers for opportunistic prediction of future cardiovascular events and mortality in an asymptomatic screening population. Lancet Digit Health 2020.
8. Pickhardt PJ, Graffy PM, Zea R, et al. Opportunistic screening for metabolic syndrome in asymptomatic adults utilizing fully automated abdominal CT-based biomarkers. AJR American journal of roentgenology 2020 Jun 29 (Epub ahead of print).
9. Pickhardt PJ, Graffy PM, Zea R, et al. Automated abdominal CT biomarkers for opportunistic prediction of future major osteoporotic fractures in asymptomatic adults. Radiology 2020 Aug 11 (Epub ahead of print).
10. Boutin RD, Kaptuch JM, Bateni CP, Chalfant JS, Yao L. Influence of IV Contrast Administration on CT Measures of Muscle and Bone Attenuation: Implications for Sarcopenia and Osteoporosis Evaluation. Am J Roentgenol 2016;207:1046–54.
11. Pickhardt PJ, Lauder T, Pooler BD, et al. Effect of IV contrast on lumbar trabecular attenuation at routine abdominal CT: correlation with DXA and implications for opportunistic osteoporosis screening. Osteoporosis Int 2016;27:147–52.
12. Pompe E, Willemink MJ, Dijkhuis GR, Verhaar HJ, Mohamed Hoesein FA, de Jong PA. Intravenous contrast injection significantly affects bone mineral density measured on CT. European radiology 2015;25:283–9.
13. Burns JE, Yao J, Chalhoub D, Chen JJ, Summers RM. A Machine Learning Algorithm to Estimate Sarcopenia on Abdominal CT. Acad Radiol 2019.
14. Sandfort V, Yan K, Pickhardt PJ, Summers RM. Data augmentation using generative adversarial networks (CycleGAN) to improve generalizability in CT segmentation tasks. Sci Rep 2019;9:16884.
15. Summers RM, Baecher N, Yao JH, et al. Feasibility of Simultaneous Computed Tomographic Colonography and Fully Automated Bone Mineral Densitometry in a Single Examination. J Comput Assist Tomogr 2011;35:212–6.
16. Yao JH, Burns JE, Forsberg D, et al. A multi-center milestone study of clinical vertebral CT segmentation. Comput Med Imaging Graph 2016;49:16–28.
17. Yao JH, O'Connor SD, Summers RM. Automated spinal column extraction and partitioning. 3rd IEEE International Symposium on Biomedical Imaging: Macro to Nano, Vols 1–32006:390–3.